Bioorthogonal Chemistry Hot Paper

DOI: 10.1002/ange.201406045

Super-Resolution Imaging of Plasma Membrane Glycans**

Sebastian Letschert, Antonia Göhler, Christian Franke, Nadja Bertleff-Zieschang, Elisabeth Memmel, Sören Doose, Jürgen Seibel,* and Markus Sauer**

Abstract: *Much of the physiology of cells is controlled by the spatial organization of the plasma membrane and the glycosylation patterns of its components, however, studying the distribution, size, and composition of these components remains challenging. A bioorthogonal chemical reporter strategy was used for the efficient and specific labeling of membrane-associated glycoconjugates with modified monosaccharide precursors and organic fluorophores. Super-resolution fluorescence imaging was used to visualize plasma membrane glycans with single-molecule sensitivity. Our results demonstrate a homogeneous distribution of N-acetylmannosamine (ManNAc)-, N-acetylgalactosamine (GalNAc)-, and O-linked N-acetylglucosamine (O-GlcNAc)-modified plasma membrane proteins in different cell lines with densities of several million glycans on each cell surface.*

The glycosylation state of proteins controls their function, localization, and stability.[1,2] Cell-surface glycans are involved in many cell–cell recognition processes, as well as tumor development, and they reflect the developmental stage and the transformation state of a cell.[3–5] Visualization of the glycoprotein patterns in plasma membranes with regard to diseases could thus pave the way for the development of refined diagnostic tools.

However, until now two obstacles have impeded the exploitation of quantitative data concerning the architecture of membrane-associated glycoproteins: the difficulty of selective and efficient labeling of glycosylated membrane proteins, and the resolution limit of optical microscopy. This is of special importance considering the existence of confined plasma membrane compartments, that is, nanodomains or clusters with a supposed size of 5–300 nm that are required for subcompartmentalization and associated functions.[6–10] Recently, the difficulty in labeling glycans by traditional molecular and cell biology techniques has been overcome by the introduction of a bioorthogonal chemical reporter strategy termed "click chemistry".[11]

Herein, the tolerance of mammalian cells to small modifications of monosaccharide precursors is exploited. Upon cellular uptake, azido- or alkyne-modified monosaccharides are covalently incorporated by the biosynthetic machinery into the substrates of glycosyltransferases to create non-native glycans. Once incorporated into components of the cell surface, these azido- or alkyne-modified glycans can be covalently labeled with alkyne- or azido-modified fluorophores, respectively, to form triazole-linked products for the in vitro and in vivo imaging of various glycoproteins.[12–14]

In our study, we combined click chemistry for labeling and super-resolution fluorescence microscopy for visualization of membrane-associated glycoproteins with subdiffraction resolution. For the metabolic labeling of sialic acid containing and mucin-type O-linked glycans, we used analogues of their biosynthetic precursors *N*-acetylmannosamine (ManNAc), and *N*-acetylgalactosamine (GalNAc), respectively; O-GlcNAc-modified plasma membrane proteins were labeled by using a GlcNAc analogue in human osteosarcoma (U2OS) and neuroblastoma (SK-M-NC) cell lines. For subdiffraction resolution fluorescence imaging with single-molecule sensitivity, we used *direct* stochastic optical reconstruction microscopy (*d*STORM).[15–17]

Since the biosynthetic machinery tolerates the addition of chemical reporters to the N-acyl group, we fed cells with the peracetylated monosaccharides *N*-azidoacetylmannosamine (Ac_4ManNAz), *N*-azidoacetylgalactosamine (Ac_4GalNAz), and *N*-azidoacetylglucosamine (Ac_4GlcNAz), which are incorporated into cell-surface glycans upon cell permeation and deacetylation.[12–14] Ac_4ManNAz and Ac_4GalNAz have been used to visualize sialic acids and mucin-type O-linked glycans in different cell types as well as in living mice and zebrafish.[12–14] Ac_4GlcNAz is modified by the GlcNAc salvage pathway enzymes to give uridine diphosphate (UDP)-GlcNAz, which is used as a substrate by the intracellular cytosolic O-GlcNAc transferase (OGT). The resulting modification with O-GlcNAc modulates signaling and regulates protein expression, degradation, and trafficking.[12–14] O-GlcNAc addition is catalyzed by a recently discovered epidermal growth factor (EGF) domain specific O-linked GlcNAc transferase (EOGT).

In a first set of experiments, we optimized the labeling of neuroblastoma cells with different azidoacetyl monosaccharides and alkyne-bearing Alexa Fluor 647 by applying Cu^I-catalyzed azide–alkyne cycloaddition in the absence and

[*] S. Letschert, Dr. A. Göhler, C. Franke, Priv.-Doz. Dr. S. Doose, Prof. Dr. M. Sauer
Department of Biotechnology & Biophysics
Julius Maximilian University Wuerzburg
Am Hubland, 97074 Würzburg (Germany)
E-mail: soeren.doose@uni-wuerzburg.de
m.sauer@uni-wuerzburg.de
Homepage: http://www.super-resolution.de
N. Bertleff-Zieschang, E. Memmel, Prof. Dr. J. Seibel
Institute of Organic Chemistry
Julius Maximilian University Wuerzburg
Am Hubland, 97074 Würzburg (Germany)
E-mail: seibel@chemie.uni-wuerzburg.de

[**] We thank L. Pliess and P. Geßner for assistance in cell culture. This work was supported by the Biophotonics Initiative of the Bundesministerium für Bildung und Forschung (grants 13N11019 and 13N12507, M.S.), the Deutsche Forschungsgemeinschaft (DFG SA829/13-1 to M.S. and DFG Se 1410/6-1 to J.S.) and the Universität Bayern e.V. (E.M.), FCI (N.B.-Z.), ISF and IRG (S.D.).

Supporting information for this article is available on the WWW under http://dx.doi.org/10.1002/anie.201406045.

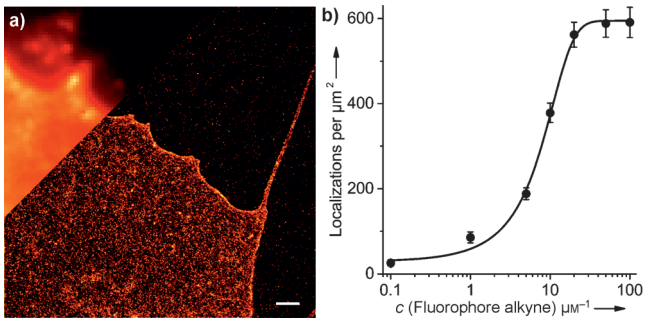

Figure 1. Membrane glycans of SK-N-MC neuroblastoma cells stained through the metabolic incorporation of azido-sugar analogues followed by copper-catalyzed azide–alkyne cycloaddition (CuAAC). a) A standard fluorescence image (upper left corner) and a high-resolution *d*STORM image (main image) of Ac_4GalNAz-treated neuroblastoma cells stained with alkyne-bearing Alexa Fluor 647. b) Localization densities of Ac_4GlcNAz-treated neuroblastoma cells for different alkyne–fluorophore concentrations. At an alkyne–fluorophore concentration of about 20 μM, the number of localizations per unit of membrane area as determined by *d*STORM becomes saturated. Scale bar: 1 μm.

presence of Cu^I and the Cu^I-stabilizing reagent Tris(3-hydroxypropyltriazolylmethyl)amine (THPTA). Cells were incubated with 25 μM aqueous solutions of modified monosaccharides in their culture medium for two days and then labeled and fixed in 4% formaldehyde with 0.2% glutaraldehyde at 25 °C to minimize the lateral diffusion of membrane molecules (Figure 1, and Figures S1, S2 in the Supporting Information).[18] A fluorophore concentration of 20 μM and an incubation time of 5 min proved to be sufficient for efficient labeling in the presence of Cu^I and THPTA (Figure 1b). Higher fluorophore concentrations do not result in higher labeling efficiencies.

The resulting *d*STORM images of Ac_4ManNAz-, Ac_4GalNAz-, and Ac_4GlcNAz-derivatized plasma membrane proteins demonstrate substantially improved resolution compared to wide-field fluorescence images and reveal the localization of single glycans homogeneously distributed over the entire basal plasma membrane of U2OS and SK-*N*-MC cells (Figure 1, Figure 2, and Figure S3 in the Supporting Information). The use of blocking agents (e.g., bovine serum albumin) to reduce unspecific binding of the fluorophores to the surface was not necessary. In control experiments, the number of non-specific localizations was found to be less than 1% (Figure S4 in the Supporting Information). To exclude the influence of the addition of copper ions and THPTA on the distribution of glycoconjugates on the basal plasma membrane, we performed copper-free experiments with Alexa Fluor 647 conjugated to dibenzocyclooctyne (DIBO) for strain-promoted azide–alkyne cycloaddition. Furthermore, we imaged the apical membrane of cells by *d*STORM to investigate the influence of the proximal coverslip. The resulting *d*STORM images appear identical and display homogeneously distributed glycans in the apical plasma membrane as well (Figure S5 in the Supporting Information). To extract reliable estimates for localization densities, 12–32 cells were imaged in all experiments and averaged data are presented (Figure 2a). Interestingly, we do not see any characteristic glycan nanodomains or clusters as have been identified in recent super-resolution imaging studies of membrane proteins.[9,10,19–21] The calculation of Ripley's K-function and nearest-neighbor distance distributions only reveals characteristic clusters on the 25 nm length scale that originate from the repeated localization of a single fluorophores (Figure S6 in the Supporting Information). Ripley's K-function might indicate some more clustering for GalNAz and ManNAz glycoconjugates when compared with simulated data for complete spatial randomness. However, no characteristic length scale could reproducibly be identified either visually or by statistical analysis (Figure S6 in the Supporting Information).

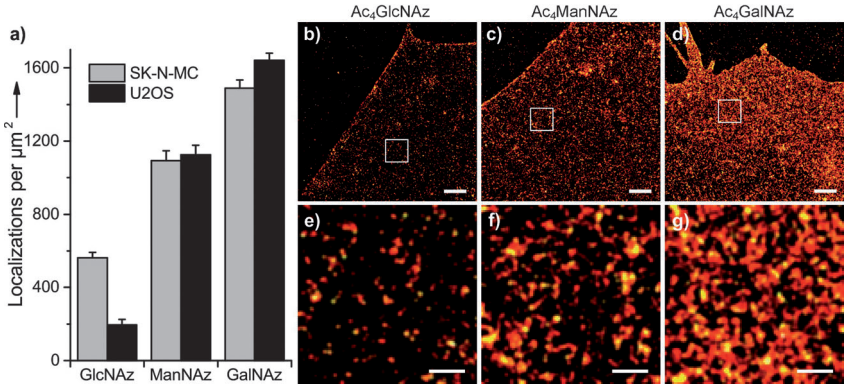

Figure 2. Super-resolution imaging and analysis of cell-surface glycoproteins. SK-N-MC neuroblastoma cells and U2OS cells were fed with one of the reactive azido sugars (Ac_4GlcNAz, Ac_4ManNAz, or Ac_4GalNAz) and then visualized and analyzed by click chemistry and *d*STORM. a) Localization density of membrane-associated glycans labeled with Alexa Fluor 647 (20 μM). Error bars represent the standard error of the mean of 12–32 imaged cells. b–d) *d*STORM images of glycoconjugates in the basal membrane of SK-*N*-MC neuroblastoma cells. Enlarged images of the sections in white boxes are shown in the lower panels (e–g). Scale bars: 1 μm (b–d) and 200 nm (e–g).

Our *d*STORM images further demonstrate that the plasma membranes of neuroblastoma and osteosarcoma cells exhibit the highest density of labeled glycans for GalNAz glycoconjugates, with 1500–1700 localizations per μm^2, followed by ManNAz-derived glycoconjugates, with approximately 1100 localizations per μm^2 (Figure 2a). GlcNAz glycoconjugates show the lowest density with a peculiar dependence on the investigated cell type (Figure 2a). For neuroblastoma cells, we find on average approximately 600 localizations per μm^2, whereas in osteosarcoma cells (U2OS), the density is substantially lower (Figure 2a). While Ac_4GalNAz and Ac_4ManNAz modify various glycoproteins and glycolipids, Ac_4GlcNAz modifies the extracellular epidermal growth factor (EGF)-like domain of just

a handful of membrane proteins,[22,23] thus explaining the lower localization density.

To estimate the number of localizations per fluorophore, spots with repeated localizations of isolated fluorophore-labeled glycans were grouped by using the tracking function of rapi*d*STORM.[24,25] To ensure that only single fluorophores were analyzed, we decreased the fluorophore concentration to 10 nM to give a very low labeling density (< 20 localizations μm^{-2}). Fluorescent spots that were switched on for longer than 10 frames were discarded from further analysis. The remaining spatially isolated fluorescent spots were tracked over the whole image stack (15000 frames) within a defined area (tracking radius) to determine the number of localizations per spot. In order to determine the optimal tracking radius, we varied the tracking radius between 0 and 200 nm. By using the mean values of the resulting distributions under saturation conditions, we extracted 2.7 ± 0.4 localizations per isolated fluorescent spot (Figure 3a and Figure S7 in the Supporting Information). By aligning the coordinates of the localizations for each isolated fluorescent spot to its center of mass, we generated a 2D histogram of all localizations, which resembles a Gauss distribution. The standard deviation of the Gauss function fitted to the projection in the *xy* plane reveals an average localization precision of 10.7 ± 0.1 nm (Figure 3b).

By using the value of 2.7 ± 0.4 localizations per isolated fluorescent spot, we can now estimate the density of GalNAz and ManNAz glycans on the basal plasma membrane to be approximately 600 μm^{-2} and 400 μm^{-2}, respectively. Accordingly, we estimate there to be approximately 220 μm^{-2} and 70 μm^{-2} GlcNAz glycans on the basal plasma membrane of neuroblastoma and osteosarcoma cells, respectively. With a basal plasma membrane area of approximately 2000 μm^2, these values correspond to around 5×10^6 fluorophore-labeled plasma membrane glycans per neuroblastoma cell (considering all three glycan modifications and including the apical and basal sides of the cell). Considering other studies, in which it has been estimated that derivatives of azidoacetyl monosaccharides replace only 4–56% of their natural analogues depending on the cell line used,[26,27] the plasma membrane of a single cell may easily contain over 10 million glycans.[28]

To conclude, our data demonstrate that the cell surface of mammalian cells is homogeneously covered with several million glycans. None of the glycoconjugates form plasma membrane clusters or nanodomains on the length scale of ten to several hundred nanometers. Since the spatial and temporal organization and functions of all of these mammalian glycans is diverse, super-resolution imaging methods in combination with click chemistry hold promise for a refined understanding of the essential cellular functions associated with cell-surface glycans.

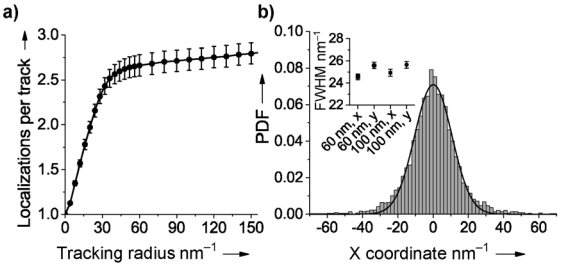

Figure 3. Quantitative analysis of *d*STORM data. a) Spots from isolated fluorophore-labeled glycans were tracked with different tracking radii over all frames. To be sure that only single fluorophores were analyzed, Ac_4GlcNAz treated SK-N-MC cells were incubated with only 10 nM alkyne-bearing Alexa Fluor 647. The curve saturates at a level of 2.68 ± 0.12 ($\pm$ SEM, $n = 12$ cells), which is the mean number of localizations per track. b) Probability density function (PDF) of all localizations belonging to a fluorescent spot, that is, an isolated fluorophore-labeled glycan, with a full width at half maximum (FWHM) of 25.2 ± 0.3 nm (mean $\pm$ standard error from the four estimates, inset), which corresponds to a localization precision (σ) of 10.7 ± 0.1 nm.

Received: June 10, 2014
Published online: August 22, 2014

Keywords: bioorthogonal chemistry · click chemistry · membrane glycans · microscopy · super-resolution imaging

[1] H. H. Freeze, *Nat. Rev.* **2006**, *7*, 537–549.
[2] G. W. Hart, M. P. Housley, C. Slawson, *Nature* **2007**, *446*, 1017–1022.
[3] K. Ohtsubo, J. D. Marth, *Cell* **2006**, *126*, 855–867.
[4] R. S. Haltiwanger, J. B. Lowe, *Annu. Rev. Biochem.* **2004**, *73*, 491–537.
[5] M. M. Fuster, J. D. Esko, *Nat. Rev. Cancer* **2005**, *5*, 526–542.
[6] K. Simons, M. J. Gerl, *Nat. Rev. Mol. Cell Biol.* **2010**, *11*, 688–699.
[7] A. Kusumi, T. K. Fujiwara, R. Chadda, M. Xie, T. A. Tsunoyama, Z. Kalay, R. S. Kasai, K. G. N. Suzuki, *Annu. Rev. Cell Dev. Biol.* **2012**, *28*, 215–250.
[8] B. F. Lillemeier, J. R. Pfeiffer, Z. Surviladze, B. S. Wilson, M. M. Davis, *Proc. Natl. Acad. Sci. USA* **2006**, *103*, 18992–18997.
[9] C. Eggeling, C. Ringemann, R. Medda, G. Schwarzmann, K. Sandhoff, S. Polyakova, V. N. Belov, B. Hein, C. von Middendorf, A. Schönle, S. W. Hell, *Nature* **2009**, *457*, 1159–1162.
[10] G. van den Bogaart, K. Meyenberg, H. J. Risselada, H. Amin, K. I. Willig, B. E. Hubrich, M. Dier, S. W. Hell, H. Grubmüller, U. Diederichsen, R. Jahn, *Nature* **2011**, *479*, 552–555.
[11] M. Boyce, C. R. Bertozzi, *Nat. Methods* **2011**, *8*, 638–642.
[12] S. T. Laughlin, C. R. Bertozzi, *Proc. Natl. Acad. Sci. USA* **2009**, *106*, 12–17.
[13] J. A. Prescher, D. H. Dube, C. R. Bertozzi, *Nature* **2004**, *430*, 873–877.
[14] S. T. Laughlin, J. M. Baskin, S. L. Amacher, C. R. Bertozzi, *Science* **2008**, *320*, 664–667.
[15] M. Heilemann, S. van de Linde, M. Schüttpelz, R. Kasper, B. Seefeldt, A. Mukherjee, P. Tinnefeld, M. Sauer, *Angew. Chem.* **2008**, *120*, 6266–6271; *Angew. Chem. Int. Ed.* **2008**, *47*, 6172–6176.
[16] S. van de Linde, A. Löschberger, T. Klein, M. Heidbreder, S. Wolter, M. Heilemann, M. Sauer, *Nat. Protoc.* **2011**, *6*, 991–1009.
[17] P. Zessin, K. Finan, M. Heilemann, *J. Struct. Biol.* **2012**, *177*, 344–348.
[18] K. A. K. Tanaka, K. G. N. Suzuki, Y. M. Shirai, S. T. Shibutani, M. S. M. Miyahara, H. Tsuboi, M. Yahara, A. Yoshimura, S. Mayor, T. K. Fujiwara, A. Kusumi, *Nat. Methods* **2010**, *11*, 865–866.

[19] J. J. Sieber, K. I. Willig, C. Kutzner, C. Gerding-Reimers, B. Harke, G. Donnert, B. Rammner, C. Eggeling, S. W. Hell, H. Grubmüller, Th. Lang, *Science* **2007**, *317*, 1072 – 1076.
[20] H. Mizuno, M. Abe, P. Dedecker, A. Makino, S. Rocha, Y. Ohno-Iwashita, J. Hofkens, T. Kobayashi, T. Miyawaki, *Chem. Sci.* **2011**, *2*, 1548 – 1553.
[21] D. J. Williamson, D. M. Owen, J. Rossy, A. Magenau, M. Wehrmann, J. J. Gooding, K. Gaus, *Nat. Immunol.* **2011**, *12*, 655 – 662.
[22] Y. Sakaidani, T. Nomura, A. Matsuura, M. Ito, E. Suzuki, K. Murakami, D. Nadano, T. Matsuda, K. Furukawa, T. Okajima, *Nat. Commun.* **2011**, *2*, 583.
[23] J. F. Alfaro, C.-X. Gong, M. E. Monroe, J. T. Aldrich, T. R. W. Clauss, S. O. Purvine, Z. Wang, D. G. Camp, J. Shabanowitz, P. Stanley, G. W. Hart, D. F. Hunt, F. Yang, R. D. Smith, *Proc. Natl. Acad. Sci. USA* **2012**, *109*, 7280 – 7285.
[24] S. Wolter, M. Schüttpelz, M. Tscherepanow, S. van de Linde, M. Heilemann, M. Sauer, *J. Microsc.* **2010**, *237*, 12 – 22.
[25] S. Wolter, A. Löschberger, T. Holm, S. Aufmkolk, M.-C. Dabauvalle, S. van de Linde, M. Sauer, *Nat. Methods* **2012**, *9*, 1040 – 1041.
[26] S. J. Luchansky, S. Argade, B. K. Hayes, C. R. Bertozzi, *Biochemistry* **2004**, *43*, 12358 – 12366.
[27] P. V. Chang, X. Chen, C. Smyrniotis, A. Xenakis, T. Hu, C. R. Bertozzi, P. Wu, *Angew. Chem.* **2009**, *121*, 4090 – 4093; *Angew. Chem. Int. Ed.* **2009**, *48*, 4030 – 4033.
[28] R. D. Cummings, J. M. Pierce, *Chem. Biol.* **2014**, *21*, 1 – 15.